NASA/TM-1998-206929

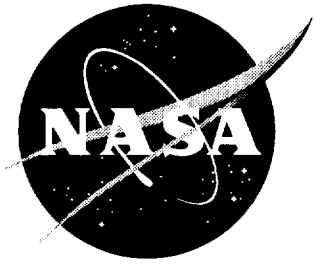

Stress Ratio Effects on Crack Opening Loads and Crack Growth Rates in Aluminum Alloy 2024

William T. Riddell and Robert S. Piascik
Langley Research Center, Hampton, Virginia

February 1998

The NASA STI Program Office ... in Profile

Since its founding, NASA has been dedicated to the advancement of aeronautics and space science. The NASA Scientific and Technical Information (STI) Program Office plays a key part in helping NASA maintain this important role.

The NASA STI Program Office is operated by Langley Research Center, the lead center for NASA's scientific and technical information. The NASA STI Program Office provides access to the NASA STI Database, the largest collection of aeronautical and space science STI in the world. The Program Office is also NASA's institutional mechanism for disseminating the results of its research and development activities. These results are published by NASA in the NASA STI Report Series, which includes the following report types:

- TECHNICAL PUBLICATION. Reports of completed research or a major significant phase of research that present the results of NASA programs and include extensive data or theoretical analysis. Includes compilations of significant scientific and technical data and information deemed to be of continuing reference value. NASA counter-part of peer reviewed formal professional papers, but having less stringent limitations on manuscript length and extent of graphic presentations.

- TECHNICAL MEMORANDUM. Scientific and technical findings that are preliminary or of specialized interest, e.g., quick release reports, working papers, and bibliographies that contain minimal annotation. Does not contain extensive analysis.

- CONTRACTOR REPORT. Scientific and technical findings by NASA-sponsored contractors and grantees.

- CONFERENCE PUBLICATION. Collected papers from scientific and technical conferences, symposia, seminars, or other meetings sponsored or co-sponsored by NASA.

- SPECIAL PUBLICATION. Scientific, technical, or historical information from NASA programs, projects, and missions, often concerned with subjects having substantial public interest.

- TECHNICAL TRANSLATION. English-language translations of foreign scientific and technical material pertinent to NASA's mission.

Specialized services that help round out the STI Program Office's diverse offerings include creating custom thesauri, building customized databases, organizing and publishing research results ... even providing videos.

For more information about the NASA STI Program Office, you can:

- Access the NASA STI Program Home Page at http://www.sti.nasa.gov/STI-homepage.html

- E-mail your question via the Internet to help@sti.nasa.gov

- Fax your question to the NASA Access Help Desk at (301) 621-0134

- Phone the NASA Access Help Desk at (301) 621-0390

- Write to:
  NASA Access Help Desk
  NASA Center for AeroSpace Information
  800 Elkridge Landing Road
  Linthicum Heights, MD 21090-2934

NASA/TM-1998-206929

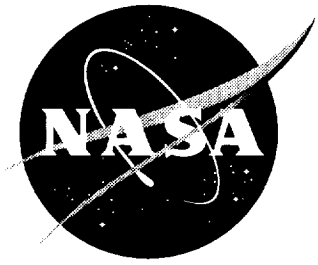

Stress Ratio Effects on Crack Opening Loads and Crack Growth Rates in Aluminum Alloy 2024

William T. Riddell and Robert S. Piascik
Langley Research Center, Hampton, Virginia

National Aeronautics and
Space Administration

Langley Research Center
Hampton, Virginia 23681-2199

February 1998

Available from the following:

NASA Center for AeroSpace Information (CASI)
800 Elkridge Landing Road
Linthicum Heights, MD 21090-2934
(301) 621-0390

National Technical Information Service (NTIS)
5285 Port Royal Road
Springfield, VA 22161-2171
(703) 487-4650

ABSTRACT:

The effects of stress ratio (R) and crack-opening behavior on fatigue crack growth rates (da/dN) for Aluminum Alloy (AA) 2024-T3 were investigated using constant-ΔK testing, closure measurements, and fractography. Fatigue crack growth rates were obtained for a range of ΔK and stress ratios. Results show that constant ΔK fatigue crack growth for R ranging from near 0 to near 1 is divided into three regions. In Region I, at low R, da/dN increases with increasing R. In Region II, at intermediate R, fatigue crack growth rates are relatively independent of R. In Region III, at high R, further increases in da/dN are observed with increasing R.

Near-crack-tip surface closure measurements, using a new noncontact displacement method, show that Region I transient crack growth rates are a result of crack closure. Increasing fatigue surface microvoid density, coinciding with increasing da/dN for Region III fatigue crack growth, suggests that a K_{max}-dependent damage mechanism is responsible for the transient fatigue crack growth rates characteristic of Region III. For AA 2024-T3, the onset of Region III correlates with a critical value of K_{max} (13 MPa $m^{1/2}$). Region II fatigue crack growth is unaffected by both closure and K_{max} effects. In this intrinsic region, $\Delta K = \Delta K_{eff}$. Rates from this region are used to test the validity of closure measurements for Region I fatigue crack growth. Poor correlation of da/dN and ΔK_{eff} occurs when ΔK_{eff} is calculated from the fully open load obtained by the reduced strain technique. Good correlation of da/dN and ΔK_{eff} are found when ΔK_{eff} is calculated from local opening loads approximately 0.1 mm behind the crack-tip.

KEYWORDS: aluminum alloy 2024, fatigue crack growth, stress ratio, crack closure, mean stress, compliance.

Introduction

Prediction of fatigue crack growth rates is of practical interest for many applications. One common method of predicting fatigue crack growth rates is the computer code, NASGRO [1]. To predict a fatigue life using this code, an appropriate parameterized configuration is chosen from a library. Parameters are input to describe a specific configuration and boundary conditions. A material library provides parameters for a fatigue crack growth model. Stress intensity factors are calculated from equations fitted to previously obtained solutions. These stress intensity factors are then input into the fatigue crack growth model to predict crack growth rates. Crack lengths are incremented, and the stress intensity factors are recalculated for the new crack size. The current form of the crack growth model in NASGRO is such that the growth rate for a given material is a function of ΔK and stress ratio (R). In this model, stress ratio affects growth rates through plasticity-induced crack closure, the premature contact of crack faces resulting from propagation through the plastic zone wake, and when K_{max} approaches K_c. For many practical situations, most of the fatigue life of a structural component is spent in the near-threshold regime. For this reason, the near-threshold regime of fatigue crack growth is of particular interest. The fatigue crack growth rate model in NASGRO should be extended to account for first-order, near-threshold environmental effects. To accomplish this, experimental methods must exhibit enough fidelity to quantify intrinsic near-threshold and lower

Paris regime fatigue crack growth rates. Described herein is research directed at developing experimental methods for determining intrinsic fatigue crack growth rates. For the purposes of this paper, "intrinsic" refers to crack growth rates that are free from closure and other stress ratio effects.

It has been well documented that stress ratio can affect fatigue crack growth rates in both the Paris regime [2-4] and near-threshold regime [5-7] of various alloys. These stress ratio effects have been explained by crack closure [8,9]. Here, fatigue crack growth rates (da/dN) correlate with effective crack-tip stress intensity factor ($\Delta K_{eff} = K_{max} - K_{open}$). Considerable research has been performed to study crack-wake closure effects [10]. Despite this research, the effect of stress ratio and crack closure on fatigue crack growth rates is still debated. Some researchers have proposed intrinsic mechanisms to explain R dependence on fatigue crack growth rates; certain K_{max} levels are needed to induce certain growth mechanisms, thus growth rates increase with R [11-12]. Other research debates the current closure standard practices; during each fatigue cycle, damage occurs both above and below the crack opening load [13]. Near-threshold and lower Paris regime closure behavior is especially complex. As the threshold regime is approached, the significance of closure mechanisms such as roughness, oxide films, or corrosion debris increases [14-17]. Therefore, extrapolation of Paris regime closure behavior to threshold and near-threshold regime closure behavior is extremely difficult. The difficulty of making direct, accurate closure measurements and interpreting these measurements correctly [18] likely obscures all of these issues. Current philosophy may consider this debate somewhat academic, so long as a growth rate model can be fitted to experimental data. However, environmental conditions affect both crack closure levels and the intrinsic da/dN-ΔK_{eff} curve. Therefore, to accurately model the environmental effects, both crack-tip and crack-wake mechanisms must be understood and modeled separately.

Consider a fatigue crack at the minimum of a cyclic load. Portions of the crack faces may be in contact. As the load increases, the crack faces "peel," and less crack face area remains in contact [19]. Eventually, the crack faces are no longer in contact. When the crack faces are first fully open, the change in slope of the load-versus-displacement curve, *i.e.*, compliance, is that of a linear-elastic, fully-open specimen [8,9]. The change in compliance corresponding to the change from small contact between the crack faces to no contact between the crack faces can be subtle, so a technique known as "reduced strain" is employed. This technique, developed by Elber [20] magnifies changes in slope to enable the fully open load to be discerned. Other methods of interpreting opening loads from compliance information exist [21]. Most of these methods use either a fixed deviation from linearity [22], or the intersection of two slopes [23] to define an opening load. Unlike Elber's fully open load, these definitions give smeared, or averaged, opening loads. The opening loads obtained from such methods are useful and appropriate engineering tools. However, smeared or averaged opening loads are likely to limit fundamental understanding of the effects of crack closure.

As the goal of this research is to isolate near-crack-tip fatigue crack growth mechanisms, opening loads should be defined to coincide with specific, near-crack-tip events. Two specific near-crack-tip events are discussed in this paper: local opening and fully open loads. A local opening load is defined as the first load that the crack faces at a given location behind the crack tip separate. Local opening loads can change with distance behind the crack-tip and with position through-the-thickness. The variation in local opening loads with location describes the peeling of the crack faces as the load increases. The local opening loads can be defined anywhere along the crack faces where contact occurs, and are a function of measurement location. The fully open load is the lowest load where the crack is completely open. The fully open load is the maximum of all local opening loads, and corresponds to Elber's definition of opening load.

In typical fatigue crack growth rate testing, ΔK is varied while either R or K_{max} is kept constant. Such standard tests can produce data relatively quickly over many orders of magnitude of crack growth rates. However, test methods where growth rates change orders of magnitude might not be sensitive to important near-threshold growth rate transients. Crack-wake effects, such as closure, can vary with load history [5]. In this regard, rates from variable-ΔK testing can also vary with load history. Therefore, an alternative test procedure is adopted herein to determine intrinsic da/dN and investigate stress ratio and crack closure effects. In this procedure, testing is performed at a constant

ΔK and stress ratio. Fatigue crack growth data obtained in this manner are sensitive to subtle, yet distinct, changes in fatigue crack growth rates associated with changing driving force mechanisms. Furthermore, constant-ΔK tests result in controlled, constant-crack-wake history, which is necessary to study crack closure.

This paper describes a series of constant ΔK, constant R tests. Near-crack-tip and far-field closure measurements and fractography are used to study the effects of stress ratio on crack closure and fatigue crack growth rates in these tests. Crack closure and K_{max} effects are both seen to affect fatigue crack growth rates, depending on ΔK and R. These effects are used to divide fatigue crack growth behavior for AA 2024-T3 into distinct regions on a ΔK-R map. Intrinsic fatigue crack growth behavior occurs when neither closure nor K_{max} effects are present. Intrinsic fatigue crack growth rates are used to test the validity of ΔK_{eff} as a predictor of stress ratio effects on closure-affected fatigue crack growth rates.

Experimental Procedure

A computer-controlled servohydraulic test system was used to perform automated, K-controlled tests. These tests were performed on AA 2024-T3 in the L-T orientation. Material properties for this alloy are shown in Table 1. All fatigue crack growth tests were conducted using pin-loaded extended compact tension specimens [24], as shown in Figure 1. Cyclic fatigue loads were applied at 11 Hz. Either front-face or back-face compliance-based methods were used to monitor crack length and adjust applied loads accordingly [25]. Optical measurements of crack length were used to validate compliance-based measurements at the beginning and end of each test. For the configurations considered, the apparent toughness (as opposed to K_{Ic}) can be described by Newman's two parameter fracture criterion [26], and is a function of crack length. Fatigue testing was performed at crack-length-to-width ratios (a/W) between 0.30 and 0.55 to minimize the effect of varying apparent toughness on high-R fatigue crack growth rates [27]. Here, the apparent toughness ranges from 52 to 46 MPa $m^{1/2}$.

Table 1 Tensile properties for AA 2024-T3 tested parallel to the longitudinal direction.

σ_y (MPa)	324
σ_{ult} (MPa)	462
E (GPa)	72

Fatigue Crack Growth Rates

Typical constant-ΔK test results of crack length (a) versus number of cycles (N) is shown in Figure 2 for AA 2024-T3 at ΔK = 5.5 MPa $m^{1/2}$, R = 0.35. Crack growth rate is determined by the slope of the a-versus-N data. A typical transient behavior is seen for the first 0.2 mm of crack growth, or nine data points (open circles), in Figure 2. Here, crack growth rates increase gradually until the steady-state growth rate is achieved. The initial, non-linear a-versus-N response results from a damage state in the crack-tip process zone that is reflective of a prior load sequence, and effects of crack-wake resulting from past crack-tip process zone conditions. These transient effects are beyond the scope of this paper, other to say that they are not considered in the fatigue crack determinations. Once "current" constant-ΔK crack-tip and crack-wake conditions are fully developed, constant driving force is fully established, and steady-state da/dN is achieved. A constant growth rate is observed for approximately 0.45 mm of crack growth, the last 18 data points (closed circles). A linear regression fit of these constant-growth-rate data characterizes the crack growth rate for AA 2024-T3 (L-T) at ΔK = 5.5 MPa $m^{1/2}$, R = 0.35 in room temperature lab air under constant crack wake conditions. By confirming that steady state crack growth rate has been established, it is ensured that history effects

due to previous loading conditions are not affecting the measured fatigue crack growth rate. To establish the effect of stress ratio on d*a*/d*N*, *R* was increased incrementally at each level of constant ΔK. After each incremental increase in *R*, the crack was grown a substantial crack length increment until a new linear *a*-versus-*N* relationship (steady-state d*a*/d*N*) was verified. It is important to emphasize that each constant ΔK crack growth rate described herein represents a constant fatigue crack growth rate observed from a statistically large sampling of linear *a*-versus-*N* data. This is done purposely to ensure that crack growth and crack wake effects are truly characterized for the desired conditions.

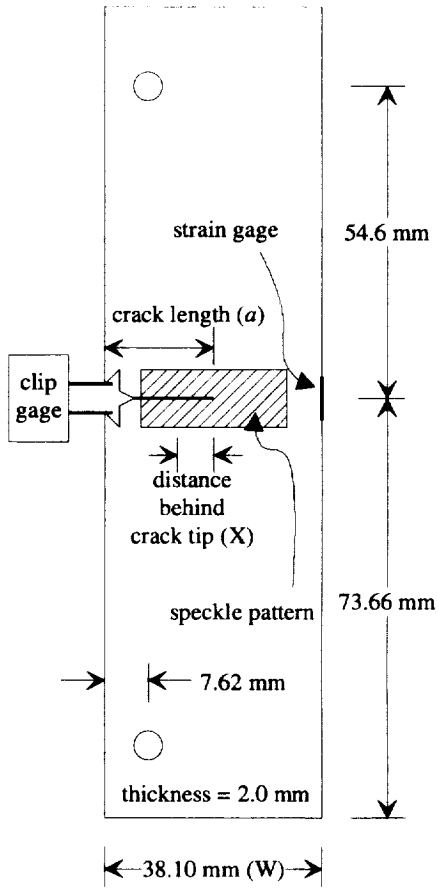

Figure 1. Extended compact tension specimen.

Near-Crack-Tip Load-Versus-Displacement Measurements

Near-crack-tip load-versus-displacement behavior is measured using a visual imaging technique, named Digital Image Displacement System (DIDS) [28]. A speckle pattern is applied to the surface of the fatigue specimen in the region surrounding the crack-tip. A series of high-magnification, near-crack-tip digital images are obtained through a long-focal-length microscope as the specimen undergoes cyclic loading. An image correlation algorithm [29] is then used to follow the movement of the speckle pattern as the applied load changes. The correlation algorithm allows sub-pixel resolution of displacement [30]. Relative displacement between a pair of points on either side of the crack face, a given distance behind the crack-tip, is determined and plotted versus load. Such traces

can be developed for a number of locations behind the crack-tip. These load-versus-relative-displacement measurements provide valuable information about near-crack-tip opening behavior during fatigue loading. Interpretation of this data will be discussed in the next section.

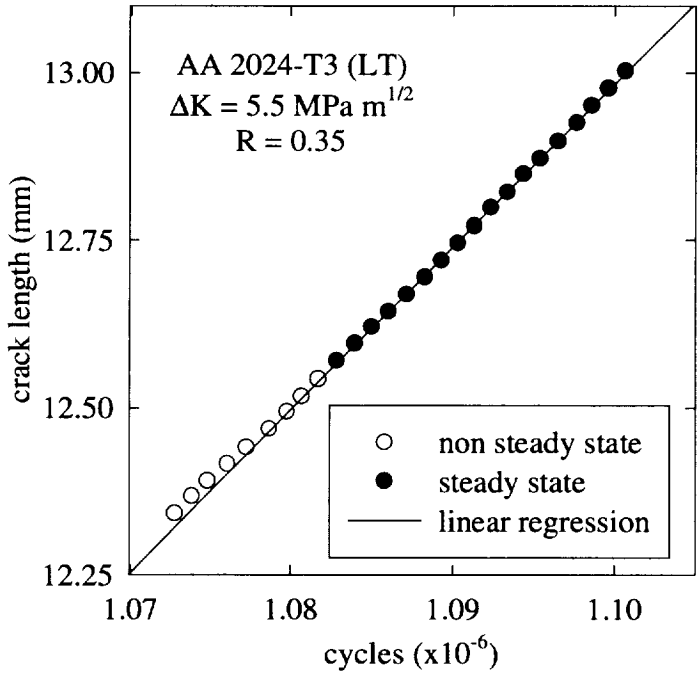

Figure 2. Typical *a* versus *N* data used to determine fatigue crack growth rate for a given ΔK and stress ratio.

Crack Opening Measurements

To determine opening loads, load-versus-displacement or load-versus-strain data, henceforth referred to as compliance data, is measured in three different locations after steady-state fatigue crack growth rates are confirmed for constant ΔK and *R* testing. The location of compliance measurements on the extended compact tension specimen are shown in Figure 1. Load-versus-displacement measurements were performed at the crack mouth using a clip gage, and at several locations less than 0.3 mm behind the crack-tip, denoted X in Figure 1, using DIDS. Load-versus-strain traces are measured at the back face using a strain gage. This compliance data is used to measure crack opening loads. Clip gage and strain gage techniques provide remote measured compliance data, while DIDS technique provides near-crack-tip surface compliance measurements.

Three near-crack-tip load-versus-displacement DIDS traces are shown in Figure 3. Each trace represents the relative displacement between a pair of points on either side of the crack face and at fixed distances (X) 0.021 mm, 0.071 mm, and 0.296 mm behind the crack-tip. For these traces, the crack-tip was at a/W = 0.22. The crack-wake and crack-front conditions for these traces were developed by 0.6 mm of crack growth under constant cyclic loading of ΔK = 3.3 MPa $m^{1/2}$, R = 0.10. Load-versus-relative-displacement records for six pairs of points, including the three represented in Figure 3, were developed from the digital images using DIDS.

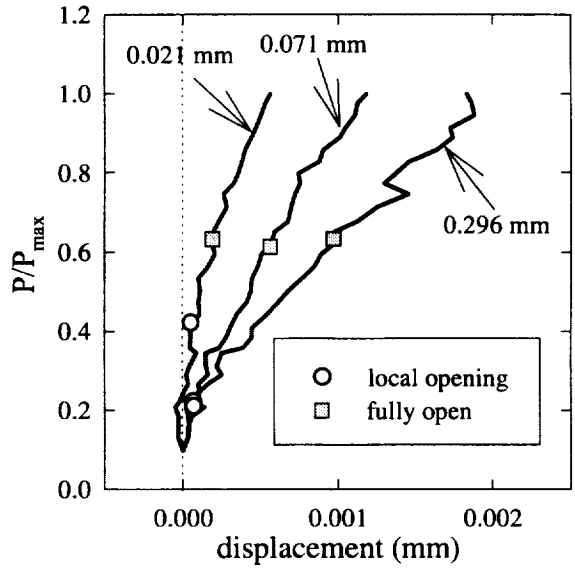

Figure 3. Load-versus-displacement traces at three locations behind a crack-tip in AA 2024, $\Delta K = 3.3$ MPa $m^{1/2}$, $R = 0.1$.

The reduced strain technique [20] was used to determine all the fully opened loads discussed in this paper. As defined, the fully open load is independent of measurement location, so near-crack-tip and remote measurements should result in the same value of fully open loads. However, the sensitivity of fully open loads is dependent on measurement location and technique [31]. Local opening loads are dependent on measurement location, so compliance measurements must be taken at (or near) part of the crack faces that are in contact during some of the load cycle, *i.e.*, near the crack-tip. There is no relative displacement between two points on opposite crack faces that are in local contact. Therefore, the load-versus-relative-displacement curve for these two points must be vertical at loads less than the local crack opening load. The local opening load for each near-crack-tip measured load-displacement trace was obtained by noting the deviation from the vertical slope at or near zero displacement (dotted line in Figure 3).

The variation of measured local opening and fully open loads as a function of distance behind the crack-tip are shown in Figure 4. The dashed line through the four highest measured fully open loads is assumed to give the true fully open level, and is independent of measurement location. The measured decrease in fully opened load 0.18 mm behind the crack-tip is believed to be caused by experimental error. The local opening load for the pair closest to the crack-tip is higher than the local opening loads discerned for the other pairs. A dotted line is drawn through the local opening loads and is extended to the fully open load at the crack-tip.

Results

Steady state fatigue crack growth data from constant ΔK, constant R tests is plotted against ΔK_{eff} calculated from both fully open and local opening loads. Local closure measurements and fractography are used to distinguish between three distinct fatigue crack growth behaviors: closure-affected, closure-free; K_{max}-independent (intrinsic); and closure-free, K_{max}-affected.

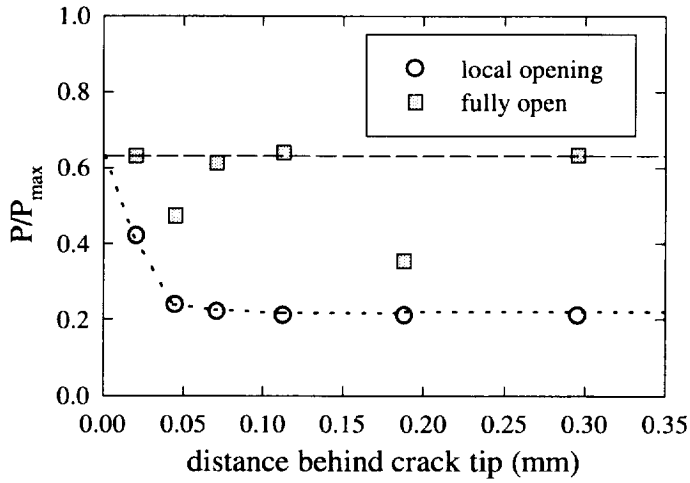

Figure 4. Local opening and fully open loads measured at various locations behind a crack-tip in AA 2024, $\Delta K = 3.3$ MPa $m^{1/2}$, $R = 0.1$.

Calculated ΔK_{eff}-versus-da/dN

When ΔK_{eff} is calculated from fully open loads, ΔK_{eff}-d*a*/d*N* data do not collapse to high-*R* d*a*/d*N*-ΔK data. Figure 5 shows ΔK_{eff} calculated from fully opened loads extracted from compliance data measured at three different locations (front face clip gage, back face strain gage, and near crack-tip) plotted versus steady state crack growth rates. Note that these results are obtained from a wide range of constant ΔK, constant *R* tests. For reference, the low- and high-*R* bounds of the d*a*/d*N*-ΔK data are shown by dashed lines. The stress ratio for the low-*R* data is 0.05 for most ΔK levels. The K_{max} for the high-*R* data is nearly equal to fracture toughness (*R* = 0.75 or greater, depending on ΔK). It is assumed that the data at high-*R* is closure free, and is an upper bound on ΔK_{eff}-d*a*/d*N* rates. Therefore, the fully open load is too high to correlate fatigue crack growth rates. As stated previously, fully open loads should be independent of measurement location. However, measured fully open loads can vary with compliance measurement location and technique; in many cases fully open loads measured using a clip gage are less than fully open loads measured by back-face strain gages or using the near-crack-tip DIDS.

When ΔK_{eff} is calculated from local opening loads, d*a*/d*N*-ΔK_{eff} data have little scatter and are bounded by high-*R* d*a*/d*N*-ΔK data. The same data are shown in Figure 6 as Figure 5, except ΔK_{eff} are calculated using the local opening load 0.10 to 0.15 mm behind the crack-tip. As seen in Figure 4, there is relatively little change in the local opening loads in the region 0.10 to 0.15 mm behind the crack-tip, so the exact location for local opening load measurement is not critical in this region.

Stress Ratio Effects on Fatigue Crack Growth Rates

Fatigue crack growth rates for AA 2024-T3 (L-T) are shown as a function of *R* for five different values of ΔK in Figure 7. Each set of d*a*/d*N* data in Figure 7 represent the result of transient-free fatigue crack growth produced under the highly controlled constant crack-wake conditions of constant ΔK, constant *R* tests. For some ΔK, data were repeated using different specimens. For these cases, the data are denoted on the plot by different symbols. For example, the results of 25 constant $\Delta K = 3.3$ MPa $m^{1/2}$ tests performed on two different specimens are shown in Figure 7(b).

The constant ΔK crack growth behavior shown in Figure 7 reveals a strong influence of *R* on fatigue crack growth rates in the range of ΔK investigated, and can be characterized into three regions: Region I, II, and III. Region I is a closure-affected region. Region II is an intrinsic, closure-free, K_{max}-independent region. Region III is a closure-free, K_{max}-dependent region. These three regions are discussed below.

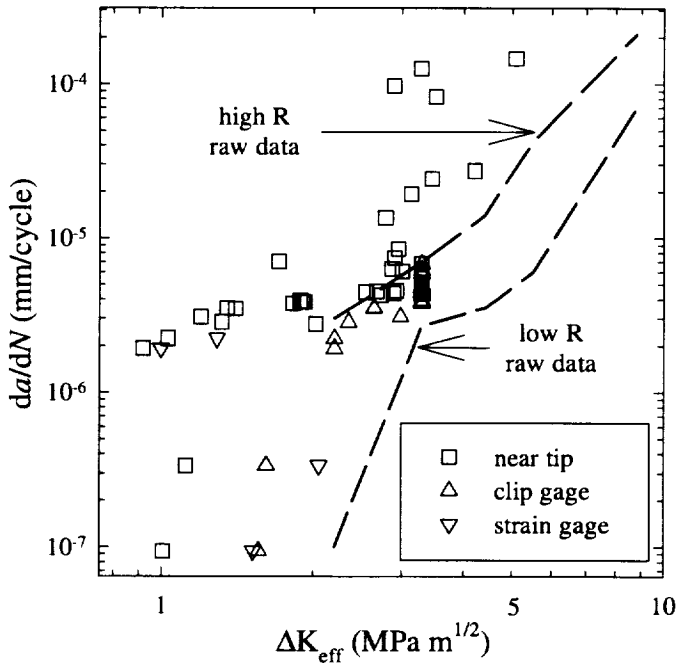

Figure 5. Fatigue crack growth rates versus ΔK_{eff} calculated using the reduced strain technique.

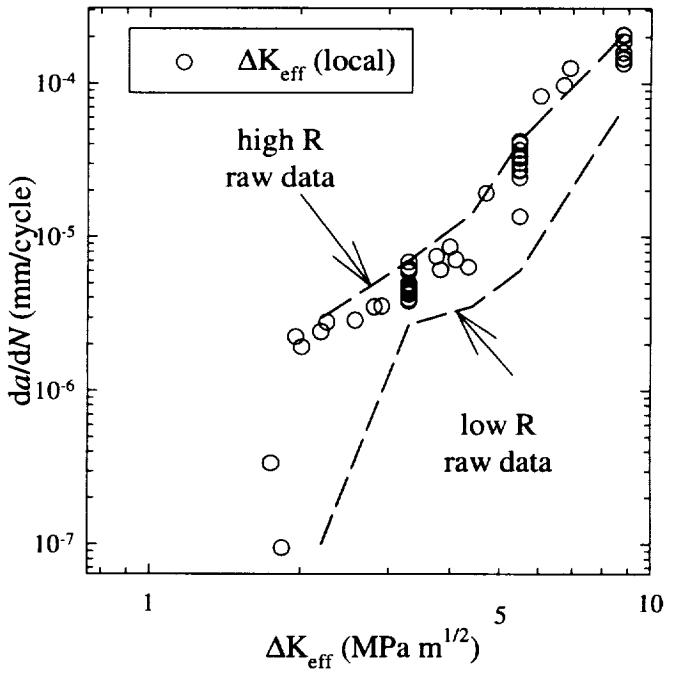

Figure 6. Fatigue crack growth rates versus ΔK_{eff} calculated using local opening loads.

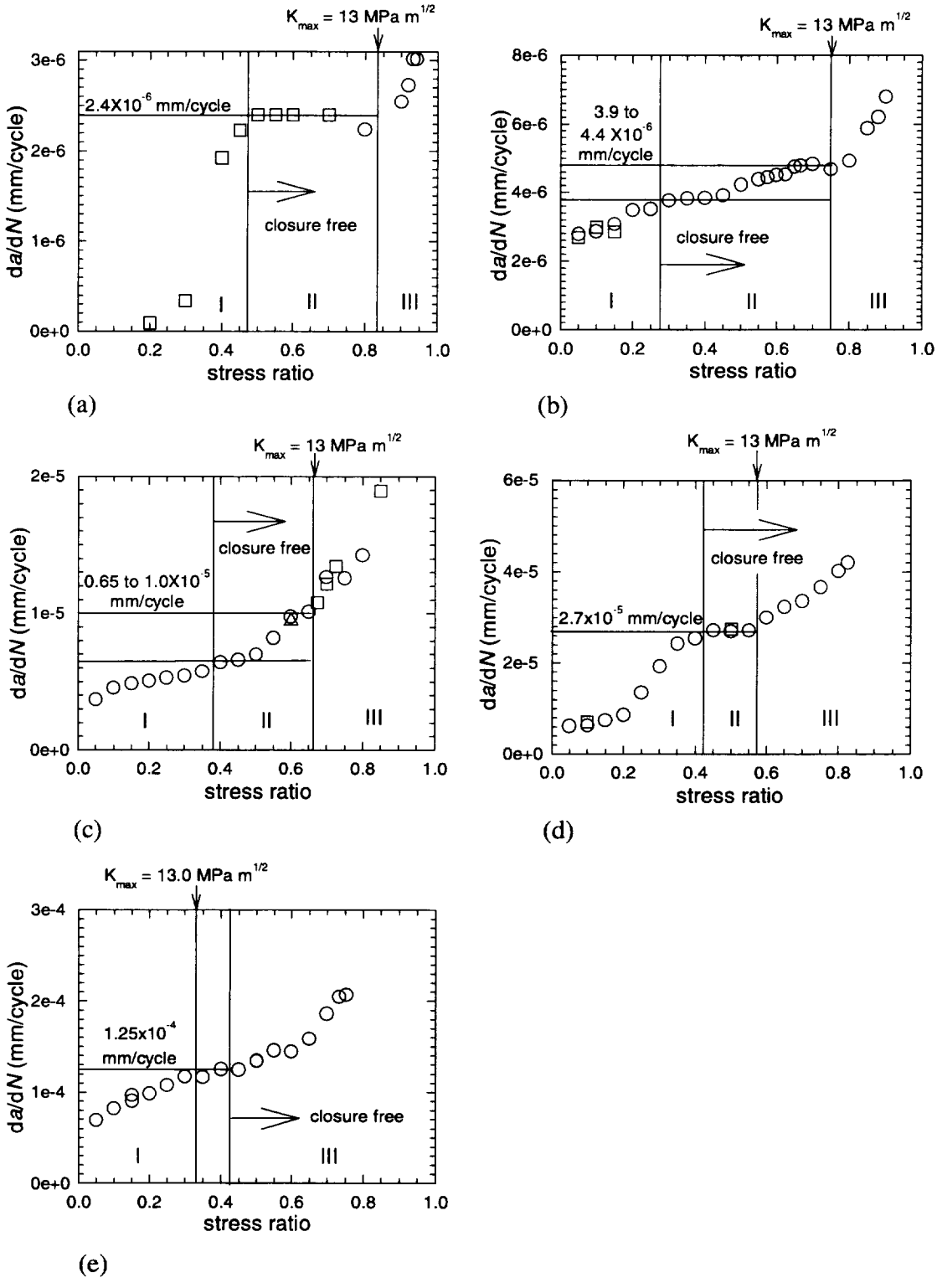

Figure 7. Steady state fatigue crack growth rates resulting from constant R constant ΔK = (a) 2.2 MPa $m^{1/2}$, (b) 3.3 MPa $m^{1/2}$, (c) 4.4 MPa $m^{1/2}$, (d) 5.5 MPa $m^{1/2}$, (e) 8.8 MPa $m^{1/2}$ tests.

The boundaries between Regions I and II were established by performing near-crack-tip local closure measurements (0.10 to 0.15 mm behind the crack-tip) during each constant ΔK test. Any tests that local closure was observed 0.10 to 0.15 mm behind the crack-tip were deemed Region I. Any tests that no closure was observed 0.10 to 0.15 mm behind the crack-tip were either Region II or Region III. Closure measurements were not made for $\Delta K = 4.4$ MPa $m^{1/2}$. The closure division for $\Delta K = 4.4$ MPa $m^{1/2}$ was identified by interpolating between test results shown in Figures 7(b) and 7(d) at $\Delta K = 3.3$ and 5.5 MPa $m^{1/2}$, respectively.

The boundary between Regions II and III represents the transition from intrinsic da/dN to a transient crack growth rate regime at higher R. Here, near-crack-tip displacement measurements verified that Region III rates are not affected by crack closure. Figures 8(a), 8(b), and 8(c) are scanning electron micrographs that show the fatigue fracture surface morphology at steady state crack growth at constant $\Delta K = 5.5$ MPa $m^{1/2}$ and constant R. Figure 8(d) shows the surface resulting from ductile tearing. Figure 8(a) reveals that the fatigue crack surface produced at $R = 0.1$ is dominated by transgranular crack growth [32]. The small (5 μm) microvoids shown in Figure 8(a) typically initiate at microstructural inhomogenieties, *i.e.*, precipitates and constituent particles, that are contained in the crack-tip process zone [33]. A comparison of Figures 8(a), 8(b), and 8(c), show that microvoids become larger and more frequent and transgranular regions become less dominant as stress ratio (K_{max}) increase from $R = 0.1$, 0.6, and 0.8, respectively. As the mechanical crack-front driving force is increased with increasing R (increasing K_{max}), more damage is produced within the crack-tip process zone. For the fatigue surface shown in Figure 8, increased crack-tip damage is associated with greater numbers of larger microvoids. At $R = 0.8$ (high K_{max}), the appearance of the fracture surface shown in Figure 8(c) approaches that of the ductile tearing, shown in Figure 8(d).

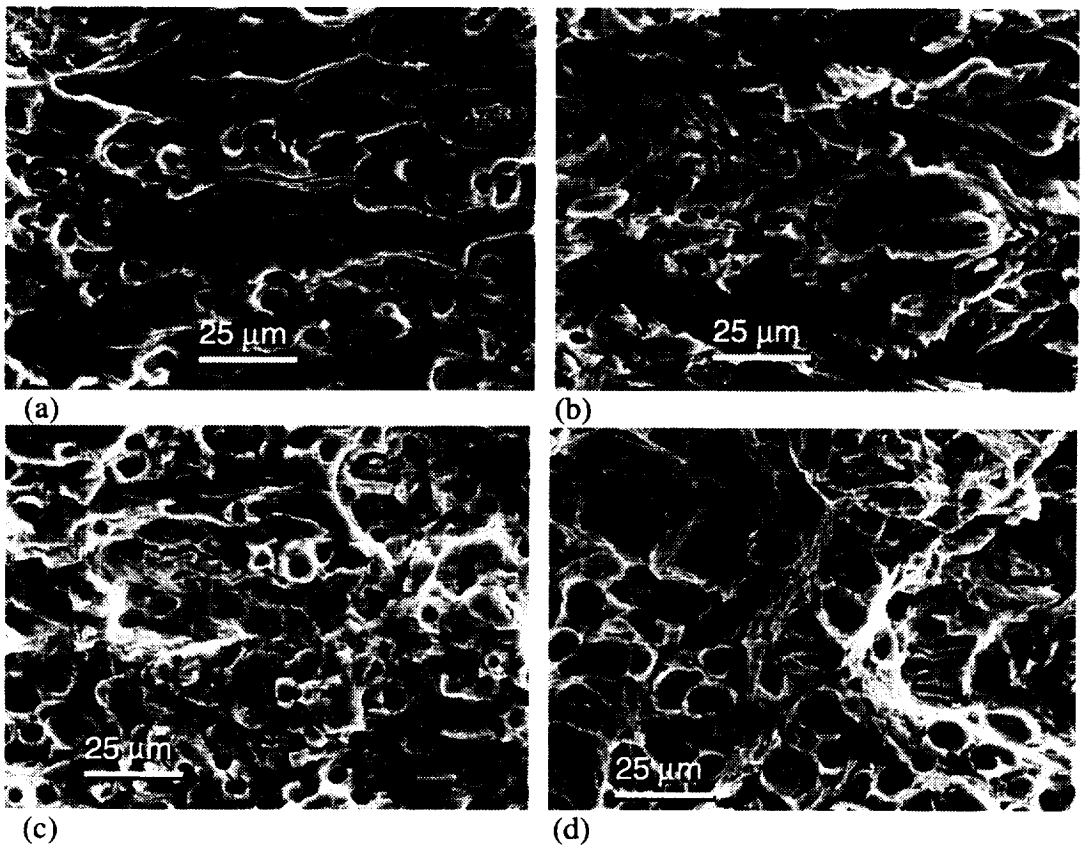

Figure 8. Micrographs of fatigue fracture surfaces for AA 2024, $\Delta K = 5.5$ MPa $m^{1/2}$ (a) $R = 0.1$, (b) $R = 0.6$, (c) $R = 0.8$, and (d) tearing.

The onset of increased microvoid damage observed in Region III is associated with a critical K_{max}. To quantify Region I, II, and III process zone damage, microvoid density determinations were made for fatigue fracture surfaces resulting from constant-ΔK steady-state crack growth. Figure 9 is a plot of microvoid density determinations for eighteen tests conducted at a constant ΔK = 5.5 MPa $m^{1/2}$ and constant *R*. A slight increase in microvoid density is observed as *R* increases from 0.05 to 0.55 (Regions I and II). The slope of the microvoid-density-versus-*R* curve for $R > 0.55$ is steeper than it is for $R < 0.55$, suggesting a critical stress ratio near $R = 0.55$ or $K_{max} \cong 13$ MPa $m^{1/2}$. The two solid lines shown in Figure 9 are the result of linear regression analysis of microvoid data for fatigue crack surfaces of *R* ranging from 0.05 to 0.55 and for *R* ranging from 0.55 to 0.84. A comparison of the microvoid density versus *R* data with the constant ΔK fatigue crack growth data in Figure 9 show that the transition for fatigue fracture surface microvoid morphology occurs at the same stress ratio and K_{max} ($R = 0.55$ and $K_{max} \cong 13$ MPa $m^{1/2}$) that separate Region II and Region III fatigue crack growth rate behavior. A further review of Figure 7 shows that a critical $K_{max} \cong 13$ MPa $m^{1/2}$ is related to transient Region III d*a*/d*N* at all levels of ΔK. As this transition is related to a distinct change in fracture surface morphology that is dependent on microstructure, the relationship and behavior observed for AA 2024-T3 might not be general to other alloys or heat treatments.

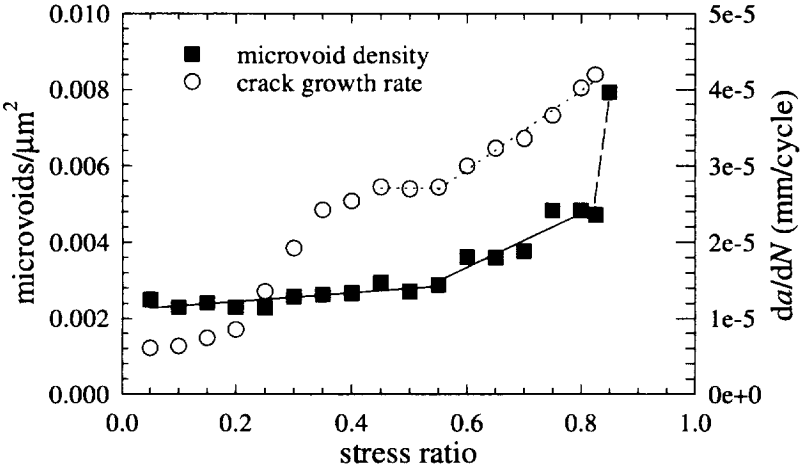

Figure 9. Relationship between stress ratio, microvoids, and crack growth rate for 2024-T3, ΔK = 5.5 MPa $m^{1/2}$.

For all levels of ΔK shown in Figure 7, the plot of d*a*/d*N* versus *R* exhibit a general shape characterized by Regions I, II, and III. Transient crack growth in Regions I and III are observed at all levels of ΔK. For ΔK = 2.2 and 5.5 MPa $m^{1/2}$, the crack growth rates in Region II form a distinct plateau. For ΔK = 3.3, and 4.4 MPa $m^{1/2}$ the plateau is less distinct. For ΔK = 4.4 MPa $m^{1/2}$, the increased crack growth rates begin when K_{max} is approximately 10 MPa $m^{1/2}$. For ΔK = 8.8 MPa $m^{1/2}$, the closure-affected/closure-free boundary occurs when $K_{max} > 13$ MPa $m^{1/2}$. Therefore, ΔK = 8.8 MPa $m^{1/2}$ does not exhibit Region II behavior. Rather, there is a Region I/III intersection for ΔK = 8.8 MPa $m^{1/2}$.

Discussion

The constant ΔK, near-threshold and lower Paris regime fatigue crack growth behavior shown in Figure 7 reveals three distinct regions for stress ratios ranging for 0 to 1.0. Near-crack-tip closure measurements confirm that Region I d*a*/d*N* is reduced from intrinsic rates by crack closure. Region II is characterized by d*a*/d*N* that is independent or nearly independent of *R*. The range of *R* that Region II occurs for varies with ΔK. The trans-plateau behavior (Region III) exhibits transient, closure-free, crack growth behavior. Here, d*a*/d*N* increases as *R* is increased, suggesting that K_{max} effects promote Region III transient crack growth behavior [34]. The three regions are further defined in Table 2.

Table 2 Regions of fatigue crack growth behavior.

Region I	closure affected	$\frac{da}{dN} = f(\Delta K_{eff})$
Region II	closure free	$\frac{da}{dN} = f(\Delta K)$
Region III	closure free, K_{max} affected	$\frac{da}{dN} = f(\Delta K, K_{max})$

Region I Fatigue Crack Growth

Figure 6 shows that a specific, near-crack-tip event, namely local closure 0.10 to 0.15 mm behind the crack-tip, explains the first order effects of R on da/dN in Region I. Figure 5 shows that the fully open load is too high to correlate fatigue crack growth rates. The three-dimensional nature of the crack closure process might explain this observation. Plasticity-induced crack closure is greater at the free surface compared to the interior of the crack front [35,36]. Simulations of three-dimensional plasticity induced crack closure [37-39] suggest that the interior part of the crack front is open while the part near the free surface is closed during a portion of the load cycle. Fatigue crack growth might occur along the open portions of the crack front while the surface is closed. The DIDS measurements are surface, as well as near-crack-tip, measurements, and are therefore especially sensitive to surface closure levels. The relationship between surface-measured phenomena and bulk closure behavior is investigated elsewhere [40].

Region III Fatigue Crack Growth

Detailed characterization of Region III-produced fatigue fracture surfaces revealed an increase in microvoid damage corresponding to the increased fatigue crack growth rates observed in Region III. These results strongly suggest a critical K_{max} above which additional crack-tip process zone damage (microvoid formation) occurs. For AA 2024-T3 sheet, a critical $K_{max} \cong 13$ MPa $m^{1/2}$ is suggested. The modest change in microvoid data for $R < 0.5$ in Figure 9 suggests a secondary or tertiary K_{max} effect for $K_{max} < 13$ MPa $m^{1/2}$. Above the critical K_{max} value, crack-tip damage is influenced by K_{max} damage modes to a much greater extent. Here, Region III crack growth rates increase by 50% compared to Region II intrinsic da/dN.

Region II Fatigue Crack Growth

Between the closure-dominated and the K_{max}-affected regions, near-threshold and lower Paris regime da/dN is nearly independent of stress ratio. Steady-state, Region II intrinsic da/dN (solid circle) for constant ΔK tests performed at 1.5, 1.7, 1.9, 2.2, 3.3, 4.4, 5.5, and 8.8 MPa $m^{1/2}$ [1], and closure-corrected, steady-state Region I da/dN for ΔK tests performed at 2.2, 3.3, 4.4, 5.5, and 8.8 MPa $m^{1/2}$ are shown in Figure 10. Closure corrected, Region I fatigue crack growth rates agree with Region II intrinsic fatigue crack growth rates. Region I fatigue crack growth rates are reduced by

[1] Intrinsic fatigue crack growth rates for 1.5, 1.7, and 1.9 MPa $m^{1/2}$ were determined by the constant ΔK, constant R fatigue crack growth rate test procedure described in the Experimental Procedure section. The Region II stress ratios for these values of ΔK were estimated based on the results shown in Figure 7(a) for $\Delta K = 2.2$ MPa $m^{1/2}$. $K_{max} = 7.3$ MPa $m^{1/2}$, $\Delta K = 2.2$ MPa $m^{1/2}$ was shown to be K_{max}-independent and closure free, so $K_{max} = 7.3$, $\Delta K = 1.5$, 1.7 and 1.9 MPa $m^{1/2}$ were assumed to be Kmax-independent and closure free as well.

crack closure. Region III fatigue crack growth rates are increased by an additional K_{max} damage mechanism. Also shown in Figure 10 are results from four variable ΔK tests: two constant R tests conducted at $R = 0.0$ and 0.5 [41], and two constant K_{max} tests conducted at K_{max} = 11 and 33 MPa $m^{1/2}$. Crack growth rates in these tests might be reduced by crack closure, increased by an additional K_{max}-induced damage mechanism, or represent intrinsic behavior. These variable ΔK test data are discussed in the next section.

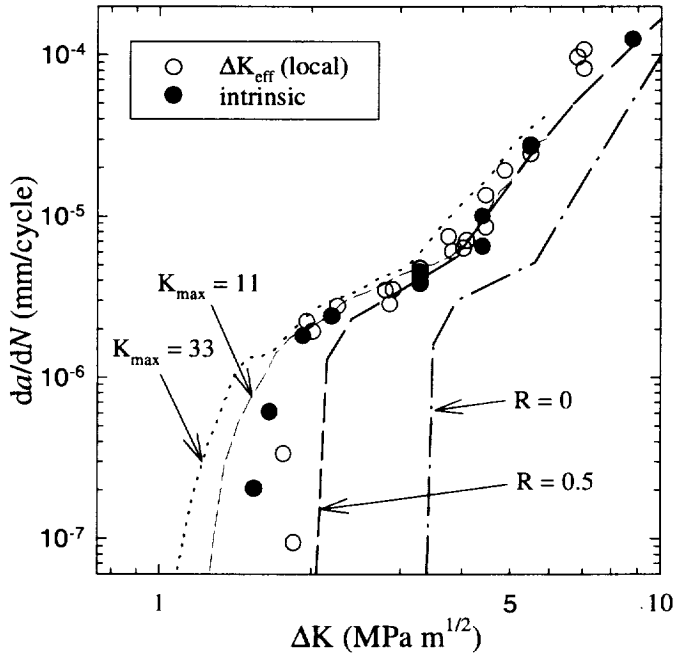

Figure 10. Closure-free, K_{max}-independent growth rates with ΔK_{eff} rates calculated from local opening loads.

Constant ΔK Maps and Variable ΔK-da/dN Testing

The Region I data corrected for local opening loads agrees well with the intrinsic, Region II growth rates. The fatigue crack growth rate data from Region II validate the use of local closure 0.10 to 0.15 mm behind the crack-tip as a means to calculate ΔK_{eff} for the range of data investigated. Further research is necessary to understand, fine tune, and generalize this algorithm. Fatigue crack growth rate data from arbitrary, high-R (Region III) tests do not correlate with ΔK_{eff}. In Region III, an alternate, K_{max}-dependent mechanism operates. This claim can be supported by the sharp transition in microvoid density shown in Figure 9. This mechanism is not accounted for in ΔK_{eff} calculations.

Each steady-state, constant-ΔK, constant-R test is plotted on the ΔK-R behavioral map shown in Figure 11. Different symbols are used to denote each behavior: Region I, Region II, Region III, and Region I/III intersection. Approximate boundaries for these regions are shown by dashed lines. These boundaries are used to delineate fatigue crack growth mechanisms operative during fatigue crack growth. The paths of variable ΔK tests, the results of which are shown in Figure 10, are shown by solid lines. Traditional variable-ΔK tests can cross behavioral boundaries, thereby changing the operative fatigue crack growth mechanisms. Fatigue data from these tests are interpreted with the aid of a behavioral map.

The behavioral map shown in Figure 11 was developed using steady-state fatigue crack growth behavior observed for constant-ΔK, constant-R tests. Data from the variable-ΔK tests are not steady-state fatigue crack growth. As such, the effective behavioral boundaries for these tests might shift from the boundaries established for steady state fatigue crack growth. Figure 11 shows that the constant-R test performed at R = 0.0 (denoted D in Figure 11) remains in Region I for the entire duration of the test. Crack closure causes fatigue crack growth rates for this test to be lower than intrinsic rates for all levels of ΔK. The constant R test performed at R = 0.5 (denoted C) is in Region III for ΔK > 6.5 MPa $m^{1/2}$, in Region II for 6.5 < ΔK < 2 MPa $m^{1/2}$ and enters Region I at ΔK ≈ 2 MPa $m^{1/2}$. The corresponding fatigue crack growth rates from this test match the intrinsic fatigue crack growth rates for ΔK from 2 to 6 MPa $m^{1/2}$. However, at low values of ΔK (less than approximately 2 MPa $m^{1/2}$) fatigue crack growth is affected by crack closure, and therefore rates fall below the intrinsic curve. Here, the onset of closure at low ΔK affects the observed fatigue threshold, even though crack closure does not affect the fatigue behavior for most of the test. The constant K_{max} = 11 MPa $m^{1/2}$ test (denoted B) also produces intrinsic rates for much of the test. However, the deviation from intrinsic rates at low ΔK indicates a transition to an additional K_{max}-driven growth mechanism, characteristic of Region III. The constant K_{max} = 33 MPa $m^{1/2}$ test (denoted A) remains in Region III for the entire duration of the test. Here, deviation from intrinsic rates is particularly noticeable when ΔK is greater than 3.3 MPa $m^{1/2}$, and when ΔK is less than 2.2 MPa $m^{1/2}$, as seen in Figure 10.

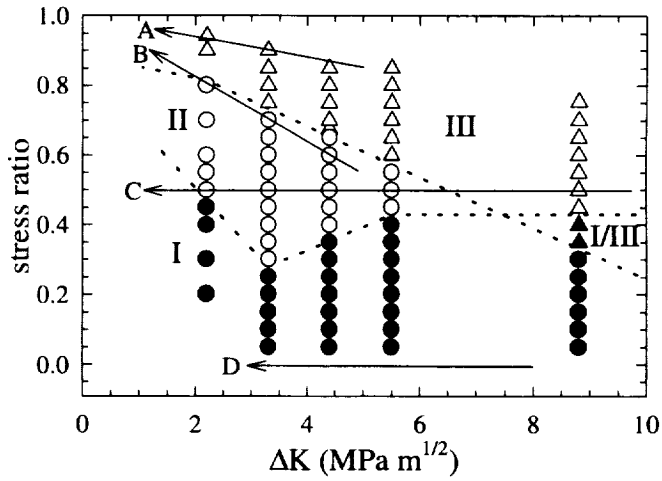

Figure 11. Paths of four variable ΔK tests, A) K_{max} = 33 MPa $m^{1/2}$, B) K_{max} = 11 MPa $m^{1/2}$, C) R = 0.5, D) R = 0.0, shown on a behavioral map for ΔK = 2024-T3 (L-T).

The deviations from intrinsic fatigue crack growth rates observed in the data from variable-ΔK tests can be interpreted with the aid of the behavioral map. However, it would be extremely difficult to discern intrinsic near-threshold fatigue crack growth rates from these tests without the aid of the behavioral map, developed through careful constant-ΔK, constant-R testing, near-crack-tip closure measurements, and fractography. For example, it is easy to foresee results from either the variable-ΔK, constant-R = 0.5 test or the variable-ΔK, constant-K_{max} = 33 MPa $m^{1/2}$ test being interpreted as intrinsic rates. However, the thresholds resulting from these two tests differ by a factor of two.

Summary and Conclusions:

A test methodology for evaluating intrinsic fatigue crack growth rates has been described. Constant-ΔK, constant-R testing, near-crack-tip closure measurements, and fractography were used to investigate the effects of stress ratio on fatigue crack growth rates. Three distinct regions of fatigue crack growth behavior were established, based on the relationship between growth rate and R for a

given ΔK. These regions are: Region I "closure-affected," Region II "closure-free, K_{max}-independent," and Region III "closure-free, K_{max}-dependent." It was shown that neither constant-R testing nor constant K_{max}-testing are adequate to determine the desired intrinsic fatigue crack growth behavior over the entire range of ΔK investigated.

Near-crack-tip closure measurements indicate that fatigue crack growth rates observed for Region I are reduced from intrinsic rates as a result of closure. Excellent agreement between steady-state Region I and Region II da/dN was found when Region I data are corrected for local opening loads measured 0.10 to 0.15 mm behind the crack-tip.

Increased fatigue crack growth rates observed in Region III cannot be accounted for by crack closure. Rather, observed changes in Region III da/dN are associated with a change in growth mechanism at increased K_{max}, as evidenced by changes in fatigue fracture surface morphology.

Acknowledgments

The authors gratefully acknowledge the help of Ms. Chelsey Gallik for the near crack-tip measurements. DIDS was developed in conjunction with Dr. Michael Sutton and his research group at the University of South Carolina. This research was performed while one author (WTR) was a National Research Council NASA Langley Research Center Research Associate.

References

[1] Forman, R.G.; Shivakumar, V.; Mettu, S.R.; Newman, J.C., Jr.: *Fatigue Crack Growth Computer Program "NASGRO" Version 3.0 User's Manual.* JSC-22267B, July 1996.

[2] Hudson, C.M.: *Effect of Stress Ratio on Fatigue Crack Growth in 7075-T6 and 2024-T3 Aluminum Alloy Specimens.* NASA TN D-5390, 1969.

[3] Ibrahim, F.K.: The Effects of Stress Level, Compressive Peak Stress and Maximum Stress Level on Fatigue Behavior of 2024-T3 Aluminum Alloy. *Fatigue and Fracture of Engineering Materials and Structures*, vol. 12, no. 1, 1989, pp. 1-8.

[4] Bilir, O.G.; Harun, M.: Effect of Stress Ratio on the Rate of Growth of Fatigue Cracks in 1100 Al-Alloy. *Engineering Fracture Mechanics*, vol. 37, no. 6, 1990, pp. 1203-1206.

[5] Phillips, E.P.: The Influence of Crack Closure on Fatigue Crack Growth Thresholds in 2024-T3 Aluminum Alloy. *Mechanics of Fatigue Crack Closure, ASTM STP 982*, J.C. Newman, Jr. and W. Elber, eds., American Society of Testing and Materials Philadelphia, PA, 1988, pp. 505-515.

[6] Couper, M.J.; Griffiths, J.R.: Effects of Crack Closure and Mean Stress on the Threshold Stress Intensity Factor for Fatigue of an Aluminum Casting Alloy. *Fatigue and Fracture of Engineering Materials and Structures*, vol. 13, no. 6, 1990, pp. 615-624.

[7] Salivar, G.C.; Heine, J.E.; Haake, F.K.: The Effect of Stress Ratio on the Near-Threshold Fatigue Crack Growth Behavior of Ti-8Al-1Mo-1V At Elevated Temperature. *Engineering Fracture Mechanics,* vol. 32, no. 5, 1989, pp. 807-817.

[8] Elber, W.: Fatigue Crack Closure Under Cyclic Tension. *Engineering Fracture Mechanics,* vol. 2, 1970, pp. 37-45.

[9] Elber, W., The Significance of Fatigue Crack Closure, *Damage Tolerance in Aircraft Structures ASTM STP 486* American Society of Testing and Materials, 1971, pp. 230-242.

[10] J.C. Newman; W. Elber, eds.: *Mechanics of Fatigue Crack Closure, ASTM STP 982,* American Society of Testing and Materials, Philadelphia, PA, 1988.

[11] Vasudevan, A.K.; Sadananda, K.; Louat, N.: Two Critical Stress Intensities for Threshold Fatigue Crack Propagation. *Scripta Metallurgica et Materialia,* vol. 28, 1993, pp. 65-70,

[12] Lal, D.N.: A Detailed Physical Analysis of the R-Effect on LEFM Fatigue Crack Growth -II. On the Combined Roles of Growth Mechanisms and Stress Ratio. *Engineering Fracture Mechanics,* vol. 55, no. 2, 1996, pp. 289-312.

[13] Chen, D.L.; Weiss, B.; Stickler, R.: The Effective Fatigue Threshold: Significance of the Loading Cycle Below the Crack Opening Load. *Fatigue,* vol. 16, 1994, pp. 485-491.

[14] Park, D.H.; Fine, M.E.: Origin of Crack Closure in the Near-Threshold Fatigue Crack Propagation of Fe and Al-3% Mg. *Fatigue Crack Growth Threshold Concepts*, D.L. Davidson and S. Suresh, eds., The Metallurgical Society of AIME, 1983, pp. 146-161.

[15] Gerberich, W.W.; Yu, W.; Esaklul, K.: Fatigue Threshold Studies in FE, Fe-Si and HSLA Steel: Part I. Effect of Strength and Surface Asperities on Closure. *Metallurgical Transactions A,* vol. 15A, 1984, pp. 875-888.

[16] Romaniv, O.N.; Tkach, A.N.; Lenets, Y.N.: Effect of Fatigue Crack Closure on Near Threshold Crack Resistance of Structural Steels. *Fatigue and Fracture of Engineering Materials and Structures,* vol. 10, no. 3, 1987, pp. 203-212.

[17] Soboyejo, W.O.; Knott, J.F.: Effects of Stress Ratio on Fatigue Crack Propagation in Q1N (HY80) Pressure Vessel Steel. *International Journal of Fatigue*, vol. 12, no. 5, 1990, pp. 403-407.

[18] Allison, J.E.; Ku, R.C.; Pompetzki, M.A.: A Comparison of Measurement Methods and Numerical Procedures for the Experimental Characterization of Fatigue Crack Closure. *Mechanics of Fatigue crack closure, ASTM STP 982*, J.C. Newman, Jr., W. Elber, eds. American Society of Testing and Materials, Philadelphia, PA, 1988, pp. 171-185.

[19] Davidson, D.L.: Plasticity Induced Fatigue Crack Closure. *Mechanics of Fatigue Crack Closure, ASTM STP 982*, J.C. Newman, Jr. and W. Elber, eds., American Society for Testing and Materials, Philadelphia, PA, 1988, pp. 44-61.

[20] Elber, W.: *Crack Closure and Crack Growth Measurements in Surface-Flawed Titanium Alloy Ti-6Al-4V.* NASA TN D-8010, 1975.

[21] Yisheng, W.; Schijve, J.: Fatigue Crack Closure Measurements on 2024-T3 Sheet Specimens. *Fatigue and Fracture of Engineering Materials and Structures,* vol. 18, no. 9, 1995, pp. 917-921.

[22] *ASTM standard E647: Standard Test Method for Measurement of Fatigue Crack Growth Rates*, American Society for Testing and Materials, 1997.

[23] Chen, D.-L.; Weiss, B.; Strickler, R.: A New Procedure for Crack Closure. *International Journal of Fatigue*, vol. 13, no. 4, 1991, pp. 327-331.

[24] Piascik, R.S.; Newman, J.C., Jr.; Underwood, J.H.: The Extended Compact Tension Specimen, *Fatigue and Fracture* of *Engineering Materials and Structures*, vol. 20, no. 4, 1997, pp. 559-563.

[25] *User's Reference Manual for Automated Fatigue Crack Growth (Compliance)*, Fracture Technology Associates, Star Route, Pleasant Valley, PA 18951, 1991.

[26] Newman, J.C., Jr.: Fracture Analysis of Various Cracked Configurations in Sheet and Plate Materials. *Properties Related to Fracture Toughness, ASTM STP 605,* American Society for Testing and Materials, 1976, pp. 104-123.

[27] Newman, J.C., Jr.: An Evaluation of the Plasticity Induced Crack Closure Concept and Measurement Methods. Advances in Fatigue Crack Closure Measurement and Analysis, ASTM STP 1343, R.C. McClung and J.C. Newman, Jr., eds. American Society for Testing and Materials, to be published.

[28] Sutton, M.A.; Zhao, W.; McNeill, S.R.; Helm, J.D.; Piascik; R.S., Riddell, W.T.: Local Crack Closure Measurements: Development of a System Using Computer Measurements and a Far-Field Microscope. submitted to *Second Symposium on Advances in Fatigue Crack Closure Measurements and Analysis*, R.C. McClung and J.C. Newman, Jr., eds., American Society for Testing and Materials, West Conshohocken, PA., to be published.

[29] Sutton, M.A.; Chao, Y.J.; Lyons, J.S.: Computer Vision Methods for Surface Deformation Measurements in Fracture Mechanics. *Novel Experimental Techniques in Fracture Mechanics, AMD-Vol.176*, ASME, 1993. pp. 203-217.

[30] Sutton, M.A.; McNeill, S.R.; Jang, J.; Babai, M.: Effect of Subpixel Image Restoration on Digital Correlation Error Estimates. *Optical Engineering,* vol. 27., no. 10, 1988, pp. 870-877.

[31] Abdel Mageed, A.M.; Pandey, R.K.; Chimadurai, R.: Effect of Measurement Location and Fatigue Loading Parameters on Crack Closure Behavior. *Material Science and Engineering,* vol. A150, 1992, pp. 43-50.

REPORT DOCUMENTATION PAGE

Form Approved
OMB No. 0704-0188

1. AGENCY USE ONLY (*Leave blank*)	2. REPORT DATE	3. REPORT TYPE AND DATES COVERED
	February 1998	Technical Memorandum

4. TITLE AND SUBTITLE
Stress Ratio Effects on Crack Opening Loads and Crack Growth Rates in Aluminum Alloy 2024

5. FUNDING NUMBERS
WU 538-02-10-01

6. AUTHOR(S)
William T. Riddell and Robert S. Piascik

7. PERFORMING ORGANIZATION NAME(S) AND ADDRESS(ES)
NASA Langley Research Center
Hampton, VA 23681-2199

8. PERFORMING ORGANIZATION REPORT NUMBER
L-17699

9. SPONSORING/MONITORING AGENCY NAME(S) AND ADDRESS(ES)
National Aeronautics and Space Administration
Washington, DC 20546-0001

10. SPONSORING/MONITORING AGENCY REPORT NUMBER
NASA/TM-1998-206929

11. SUPPLEMENTARY NOTES
W.T. Riddell: NRC, Langley Research Center

12a. DISTRIBUTION/AVAILABILITY STATEMENT
Unclassified–Unlimited
Subject Category 26 Distribution: Standard
Availability: NASA CASI (301) 621-0390

12b. DISTRIBUTION CODE

13. ABSTRACT (*Maximum 200 words*)
The effects of stress ratio (R) and crack opening behavior on fatigue crack growth rates (da/dN) for aluminum alloy (AA) 2024-T3 were investigated using constant-delta K testing, closure measurements, and fractography. Fatigue crack growth rates were obtained for a range of delta K and stress ratios. Results show that constant delta K fatigue crack growth for R ranging from near 0 to 1 is divided into three regions. In Region I, at low R, da/dN increases with increasing R. In Region II, at intermediate R, fatigue crack growth rates are relatively independent of R. In Region III, at high R, further increases in da/dN are observed with increasing R.

14. SUBJECT TERMS
Aluminum Alloy 2024; Fatigue Crack Growth; Stress Ratio; Crack Closure; Mean Stress; Compliance

15. NUMBER OF PAGES
22

16. PRICE CODE
A03

17. SECURITY CLASSIFICATION OF REPORT	18. SECURITY CLASSIFICATION OF THIS PAGE	19. SECURITY CLASSIFICATION OF ABSTRACT	20. LIMITATION OF ABSTRACT
Unclassified	Unclassified	Unclassified	

[32] Ranganathan, N.; Bouchet, B.; Petit, J.: Fractographic Aspects of the Effect of Environment on the Fatigue Crack Propagation Mechanism in a High-Strength Aluminum Alloy. *Fractography of Modern Engineering Materials: Composites and Metals, ASTM STP 948*, J.E. Masters and J.J. Au, eds., American Society for Testing and Materials, Philadelphia, 1987, pp. 424-446.

[33] Bretz, P.E.; Vasudevan, A. K.; Bucci, R.J.; Malcom, R.C.: Fatigue Crack Growth Behavior of 7XXX Aluminum Alloys Under Simple Variable Amplitude Loading. *Fracture Mechanics: Fifteenth Symposium, ASTM STP 833*, R.J. Sanford, ed., American Society for Testing and Materials, Philadelphia, PA, 1984, pp. 242-265.

[34] Clark, T.R.; Herman, W.A.; Hertzberg, R.W.; Jaccard, R.: A Technical Note: Influence of Mean Stress on Fatigue in Several Aluminum Alloys Utilizing K_{max} Threshold Procedures. *Fatigue and Fracture of Engineering Materials and Structures*, vol. 19, no. 7, 1996, pp. 949-954.

[35] Ray, S.K.; Grandt, A.F., Jr.: Comparison of Methods for Measuring Fatigue Crack Closure in a Thick Specimen. *Mechanics of Fatigue Crack Closure, ASTM STP 982,* J.C. Newman, Jr. and W. Elber, eds., American Society for Testing and Materials, Philadelphia, PA, 1988, pp. 197-213.

[36] Dawicke, D.S.; Shivakumar, K. N.; Newman, J.C.; Jr., Grandt, A.F., Jr.: An Inverse Method for the Calculation of Through-Thickness Fatigue Crack Closure Behavior. *Fracture Mechanics: Twenty Second Symposium (Vol. II), ASTM STP 1131,* S.N. Atluri; J.C. Newman, Jr.; I.S. Raju and J.S. Epstein, eds., American Society for Testing and Materials, Philadelphia, PA, 1992, pp. 46-57.

[37] Chermahini, G.R.: Shivakumar, K.N.; Newman, J.C., Jr: Three Dimensional Finite Element Simulation of Fatigue Crack Growth and Closure. Mechanics of Fatigue Crack Closure, ASTM STP 892, J.C. Newman, Jr. and W. Elber, eds., American Society for Testing and Materials, 1988, pp. 398-413.

[38] Chermahini, G.R.; Shivakumar, K.N.; Newman, J.C., Jr: Fatigue Crack Growth and Closure Behavior of Semi-Circular Elliptical Surface Flaws. International Journal of Fatigue, vol. 15, no. 4, 1993, pp. 259-263.

[39] Seshadri, B.R.; Dattaguru, B.; Ramamurthy, T.S.: Three Dimensional Elastic Plastic Finite Element Analysis of Crack Closure in CT Specimen. Contemporary Research in Engineering Science, R.C. Bodra, ed. Springer-Verlag, Berlin, 1995, pp. 491-515.

[40] Riddell, W.T.; Piascik, R.S.; Sutton, Zhao, W.; M.A.; McNeill; Helm, J.D.: Determining Fatigue Crack Opening Loads from Near-Crack-Tip Displacement Measurements. Advances in Fatigue Crack Closure Measurement and Analysis, Second Volume, ASTM STP 1343, R.C. McClung and J.C. Newman, Jr., eds. American Society for Testing and Materials, 1999.

[41] Newman, J.C., Jr.; Edwards, P.R.: *Short Crack Growth Behavior in an Aluminum Alloy - An AGARD Cooperative Test Programme.* AGARD Report No. 732, AGARD, 1988.